A candidate anti-HIV reservoir compound, auranofin, exerts a selective 'anti-memory' effect by exploiting the baseline oxidative status of lymphocytes.

B. Chirullo, R. Sgarbanti, D. Limongi, I. L. Shytaj, D. Alvarez, B. Das, A. Boé, S. Dafonseca, N. Chomont, L. Liotta, et al.

npg

A candidate anti-HIV reservoir compound, auranofin, exerts a selective 'anti-memory' effect by exploiting the baseline oxidative status of lymphocytes

B Chirullo[1,9], R Sgarbanti[2,9], D Limongi[2], IL Shytaj[1], D Alvarez[3], B Das[3], A Boe[1], S DaFonseca[4], N Chomont[4], L Liotta[5], E III Petricoin[5], S Norelli[1], E Pelosi[1], E Garaci[6,9], A Savarino*[,1,9] and AT Palamara[7,8,9]

Central memory (T_{CM}) and transitional memory (T_{TM}) CD4$^+$ T cells are known to be the major cellular reservoirs for HIV, as these cells can harbor a transcriptionally silent form of viral DNA that is not targeted by either the immune system or current antiretroviral drug regimens. In the present study, we explored the molecular bases of the anti-HIV reservoir effects of auranofin (AF), a pro-oxidant gold-based drug and a candidate compound for a cure of AIDS. We here show that T_{CM} and T_{TM} lymphocytes have lower baseline antioxidant defenses as compared with their naive counterpart. These differences are mirrored by the effects exerted by AF on T-lymphocytes: AF was able to exert a pro-differentiating and pro-apoptotic effect, which was more pronounced in the memory subsets. AF induced an early activation of the p38 mitogen-activated protein kinase (p38 MAPK) followed by mitochondrial depolarization and a final burst in intracellular peroxides. The pro-differentiating effect was characterized by a downregulation of the CD27 marker expression. Interestingly, AF-induced apoptosis was inhibited by pyruvate, a well-known peroxide scavenger, but pyruvate did not inhibit the pro-differentiating effect of AF, indicating that the pro-apoptotic and pro-differentiating effects involve different pathways. In conclusion, our results demonstrate that AF selectively targets the T_{CM}/T_{TM} lymphocyte subsets, which encompass the HIV reservoir, by affecting redox-sensitive cell death pathways.

The gold compound auranofin (AF) is a candidate drug for curing HIV infection, showing the potential to hit crucial therapeutic targets that are not accessible to the antiretroviral drugs (ARVs) currently in use.[1–5] Although ARVs are able to clear viremia and improve the immunological condition of HIV-infected individuals for prolonged time,[6] the virus rebounds to levels comparable to those observed before treatment initiation shortly after treatment is withdrawn.[6] AF is the first drug shown to induce a partially selective killing of central and transitional memory T cells (henceforth T_{CM} and T_{TM}, respectively[7]), which are pivotal carriers of HIV during conventional therapies.[8] T_{CM} and T_{TM} constitute one main viral reservoir that is long-lived and harbors dormant proviral DNA copies integrated in the genome that cannot be targeted by either the immune system or drug-based therapies. However, different stimuli can reactivate proviral DNA to produce new infectious viral particles.[9,10]

Also *in vivo* AF showed the potential to target the viral reservoir, given its ability to induce cell death in the memory T-cell compartment (recently reviewed in Badley *et al.*[1]). In this regard, we recently showed in the macaque AIDS model (i.e., rhesus macaques chronically infected with the HIV simian homolog, SIVmac251) that treatment with a drug combination consisting of ARVs and AF is able to induce a long-term reduction in the post-therapy viral set point following therapy suspension.[7,11] Importantly, the effects of AF on the memory cell subset were not associated with any detectable immune impairment *in vivo*. Moreover, we recently proved that the effects of AF can be enhanced in the context of a combined anti-reservoir therapy, inducing a drug-free remission of the disease in chronically SIVmac251-infected macaques.[12]

Despite the extensive study of gold salts conducted throughout the centuries,[13–15] a comprehensive picture of the effects and mechanism of action of AF on the immune

[1]Istituto Superiore di Sanità, Viale Regina Elena, 299, Rome, Italy; [2]Scientific Institute for Research, Hospitalization and Health Care, Università Telematica San Raffaele, Rome, Italy; [3]Department of Molecular Biology and Microbiology, Case Western Reserve University School of Medicine, Cleveland, OH, USA; [4]Vaccine and Gene Therapy Institute Florida, Port St Lucie, FL, USA; [5]Center for Applied Proteomics and Molecular Medicine, George Mason University, Manassas, VA, USA; [6]Department of Experimental Medicine and Surgery, University of Rome Tor Vergata, Rome, Italy; [7]Dept of Public Health and Infectious Diseases, Institute Pasteur Cenci Bolognetti Foundation, Sapienza University of Rome, Rome, Italy and [8]San Raffaele Pisana Scientific Institute for Research, Hospitalization and Health Care, Rome, Italy
*Corresponding author: A Savarino, Istituto Superiore di Sanità, Viale Regina Elena, 299, Rome 00161, Italy. Tel: +39 0649902305; Fax: +39 0649903561; E-mail: andrea.savarino@iss.it
[9]These authors contributed equally to this work.

system is still lacking, particularly in the CD4$^+$ T-cell compartment. It is known that AF impairs the proliferative capacity of T-lymphocytes *in vitro*[16,17] and decreases production of pro-inflammatory cytokines in macrophages and T cells.[18,19] Moreover, AF has been shown to induce intracellular oxidative stress by compromising the antioxidant defense due to the inhibition of thioredoxin reductase (TrxR).[20,21] However, the molecular pathways associated with these effects have been characterized in detail only in tumor cells, never in primary lymphocytes.[22,23]

In the present study, we show that the main antioxidant defenses of the cell decrease paralleling the lymphocyte differentiation stage. This deficiency of antioxidant defense in differentiated memory CD4$^+$ T cells is associated with increased susceptibility to a signaling cascade sparked by AF and leading to cell death. These findings suggest the molecular bases upon which the anti-reservoir effects of AF are grounded.

Results

AF exerts cytocidal and pro-differentiating effects on different lymphocyte memory T-cell compartments *in vitro*. In a previous study, we analyzed the *in vivo* and *in vitro* effects of AF[7] on CD4$^+$ T-cell subpopulations in

peripheral blood of rhesus macaques infected with SIV-mac251 and treated with antiretroviral therapy (ART) plus AF. We showed that AF induced a significant reduction in the frequency of the long-lived T_{CM}/T_{TM} cells.[7] We first aimed at confirming these effects of AF on sorted CD4$^+$ T-cell subpopulations isolated from a cohort of uninfected human donors. For this purpose, we measured, by flow cytometry, the expression of CD27, that is, a marker for long-lived phenotypes, and the frequency of Annexin V$^+$ cells, that is, a predictive marker for apoptosis. The results confirmed that AF induced CD27 downmodulation with a concomitant increase in the frequency of Annexin V$^+$ cells (Figure 1a). Annexin V staining was more pronounced in the memory compartment, including T_{CM} and T_{TM} lymphocytes, that is, the cell types that encompass the HIV-1 reservoirs ($P<0.05$, repeated measures ANOVA followed by the Newman–Keuls *post-hoc* test, five donors). These results confirm and extend those previously obtained *in vitro* in human CD4$^+$ T cells and *in vivo* in SIVmac251-infected macaques.[7]

As during the progression of HIV infection the T_{CM} and T_{TM} CD8$^+$ T cells become activated[24] and this activation correlates with disease progression,[25] we analyzed whether AF might also shorten the lifespan of the T_{CM} and T_{TM} compartments of CD8$^+$ T cells. Experiments conducted in sorted CD8$^+$ T-cell
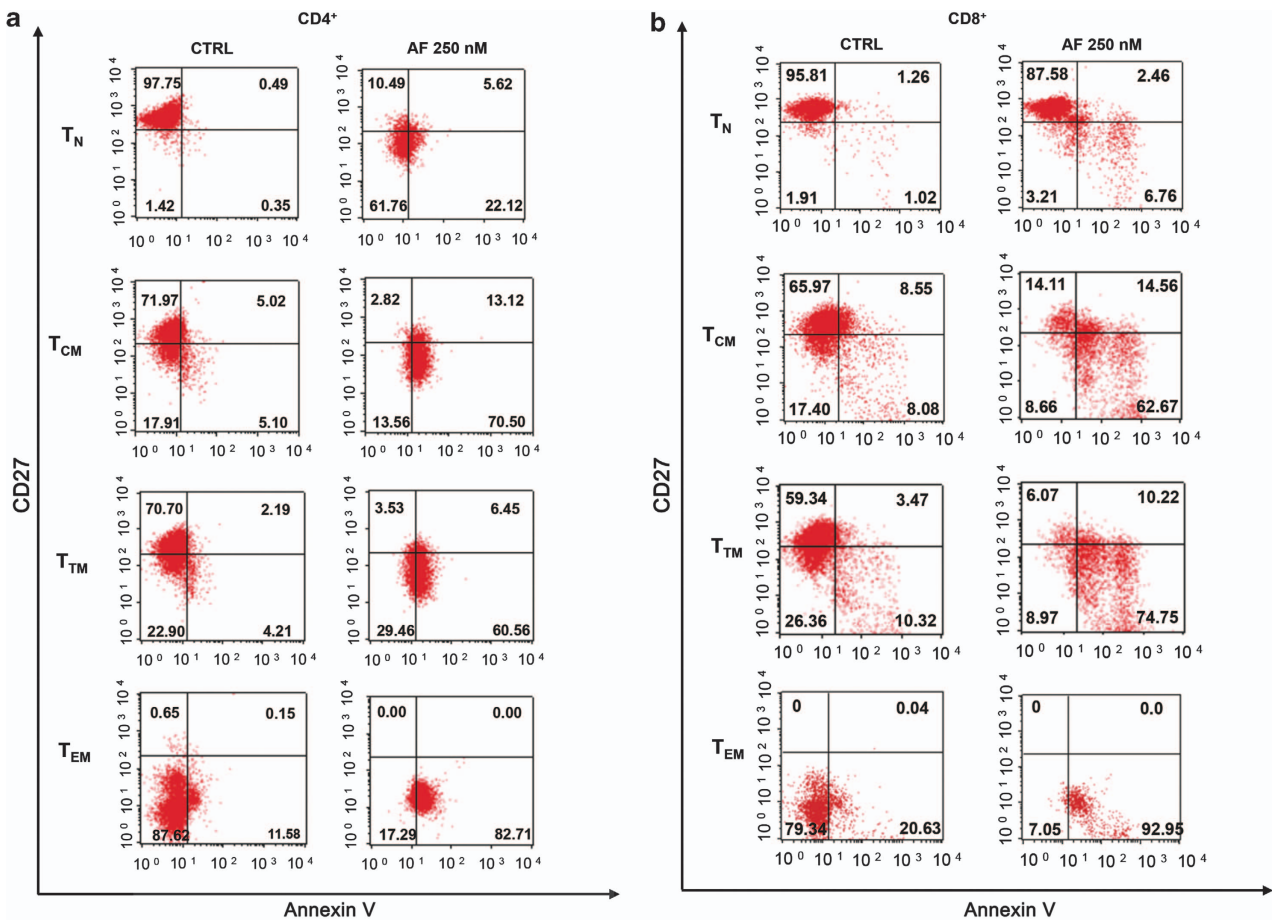
Figure 1 Dot plots showing anti-CD27 and Annexin V staining after 48 h of treatment with AF (gate on live cells) in (**a**) CD4$^+$ and (**b**) CD8$^+$ T-cell subpopulations. CD4$^+$ and CD8$^+$ T_N, T_{CM}, T_{TM} and T_{EM} T cells were separated by sorting and treated with AF at 250 nM or left untreated (gated on live CD4$^+$ T cells on the basis of the physical parameters). The dot plots show data from one representative experiment out of five (**a**) and out of three (**b**) with similar results

subpopulations showed that, similar to what was observed in CD4$^+$ T cells, CD8$^+$ T$_{CM}$, T$_{TM}$ and effector memory T (T$_{EM}$) lymphocytes succumbed more readily than the naive (T$_N$) subset to AF treatment ($P<0.05$, repeated measures ANOVA followed by the Newman–Keuls *post-hoc* test, three donors). Moreover, downmodulation of CD27 was evident in all subsets (Figure 1b). We concluded that AF exerts a pro-differentiating effect and shortens the lifespan of memory T cells independent of their CD4$^+$ or CD8$^+$ lineage.

To confirm that susceptibility to AF-induced cell death was associated with the stage of lymphocyte differentiation, we tested the effects of AF in stem cells (CD34$^+$ cells) purified from human cord blood. We stained stem cells with Annexin V after 24 and 48 h of treatment with AF. The results showed that AF had no effect on the frequency of Annexin V$^+$ cells (Supplementary Figure S1; note that CD27 is not expressed by stem cells). We conclude that the cell-death-promoting effect of AF increases in parallel to the stage of lymphocyte differentiation.

The cytocidal and pro-differentiating effects of AF are associated with the baseline oxidative status of CD4$^+$ T cells. As the pro-oxidant effects of AF are well known in the literature,[26] we analyzed, in sorted CD4$^+$ T-cell subpopulations, the baseline levels of the major marker of the intracellular redox state, that is, glutathione (GSH).[27] The results showed that GSH levels were lower in the memory cell subpopulations than in the T$_N$ compartment ($P<0.001$; Figure 2a). Repletion of GSH, however, did not inhibit the cytocidal and pro-differentiating effect of AF (data not shown), indicating that GSH is unlikely to be a direct target of AF in CD4$^+$ T cells.

To test whether this result could be extendable to the bulk of intracellular reactive thiols, we analyzed sorted CD4$^+$ T-cell subpopulations by flow cytometry, using the ThiolTracker Violet (Invitrogen Molecular Probes, Milan, Italy) (Figure 2b). We found that the total thiol content decreased in parallel to the level of lymphocyte differentiation ($P<0.05$; Spearman's correlation test, see Figure 2b).

The thiol/selenium proteins TrxRs represent another major intracellular defense against oxidative stress. AF is a well-known inhibitor of TrxRs and, in the present study, it was used at TrxR-inhibitory concentrations.[28] To test whether inhibition of these enzymes in an AF-independent manner might replicate the effect of AF, we incubated primary CD4$^+$ T cells with arsenic trioxide (As$_2$O$_3$), another well-known inhibitor of TrxRs. Results showed that As$_2$O$_3$ replicates the effect of AF at TrxR-inhibitory concentrations (i.e., 2 μM; see Figure 2c). As$_2$O$_3$ did not exert this effect at a concentration of 250 nM, that is, lower than its EC$_{50}$ on purified TrxRs (Lin *et al.*[28] data not shown). We conclude that compounds that inhibit TrxRs are able to induce both pro-differentiating and cytocidal effects in human primary CD4$^+$ T cells.

Involvement of p38 MAPK activation in AF-mediated cell death. Some of the most important signaling molecules in lymphocyte cell death and differentiation are mitogen-activated protein kinases (MAPK), a family of serine/threonine kinases.[29] The MAPK superfamily consists of different groups, one of which includes p38 MAPK,[30]

the activation of which represents one of the earliest sensors of TrxR inhibition. Incubation of CD4$^+$ T cells with AF increased the phosphorylation of p38 MAPK in Tyr182 (Figure 3a). This phosphorylation could be detected at 1 h after treatment with AF, and, to a lesser extent, at 6 and 24 h (Figure 3a).

To further confirm that p38 MAPK is involved in AF-induced lymphocyte cell death and differentiation, we tested a specific inhibitor of this protein (the pyridyl-imidazole inhibitor SB203580). Results showed that SB203580 inhibited the Annexin V stainability of T cells induced by AF and, to a lesser extent, their differentiation (Figures 3b–d). Instead, chemical inhibition of Erk1/2, another member of the MAPK super-family, using the PD98059 inhibitor, enhanced AF-mediated cell death (Supplementary Figure S2). We conclude that p38 MAPK is an important mediator of AF-induced cell death and differentiation, whereas the Erk1/2 MAPK family member delivers a survival signal in primary CD4$^+$ T cells, in line with previous evidence from AF-untreated cells.[31]

AF decreases the mitochondrial membrane potential. To further dissect the mechanism of AF-induced apoptosis, we examined the mitochondrial membrane potential (MMP, $\Delta\psi$m), a decrease of which may follow p38 MAPK activation. Changes in MMP were assessed by the fluorescence transition of the JC-1 probe, with a change from red to green fluorescence indicating a decrease in MMP (typically observed in cells undergoing apoptosis). As shown in Figure 4, treatment with AF resulted in a decrease in MMP of CD4$^+$ T cells, indicating that AF-induced apoptosis involves the mitochondrial pathway.

T$_N$ and T$_{CM}$/T$_{TM}$ CD4$^+$ lymphocytes respond to AF administration activating both common and different downstream signals involved in regulating cell survival, proliferation and differentiation. To explore the correlates of susceptibility to or protection from AF-induced cell death, we analyzed, in sorted CD4$^+$ T-cell subpopulations, the AF-induced changes of an array of proteins involved in antioxidant and pro-/anti-apoptotic pathways. Protein array analysis showed that AF prompted dramatic changes in protein expression, which, in some cases, were peculiar to the different subsets analyzed (Figures 5a–c). In all long-lived CD4$^+$ subsets, that is, T$_N$, T$_{CM}$ and T$_{TM}$, AF increased the levels of the pro-apoptotic factors Ask1 (S38 phosphorylated), p38 (Tyr180 phosphorylated, Figure 5b) and Bax/Bak (total, Figure 5c), but decreased the expression of the apoptosis-regulating factor p53 (Figure 5c). Moreover, AF increased the levels of the lymphocyte activation and differentiation factor phospho-ZAP-70(Tyr319)/SyK(Tyr352) (Figure 5c). In line with the well-known positive feedback effects induced by the presence of a specific inhibitor,[32] TrxR1 and TrxR2 were also increased in all CD4$^+$ subsets (Figure 5a). On the other hand, the mitochondrial peroxide generator, Mn^{2+} superoxide dismutase (MnSOD), was upregulated by AF only in the memory T-cell subsets (Figure 5a). No peculiar change was instead observed for the AF-treated T$_N$ subset, apart from extremely high levels of the antioxidant and anti-apoptotic enzyme TrxR2 (data not shown). As a support of the concept that susceptibility to AF-induced apoptosis increases in parallel to lymphocyte
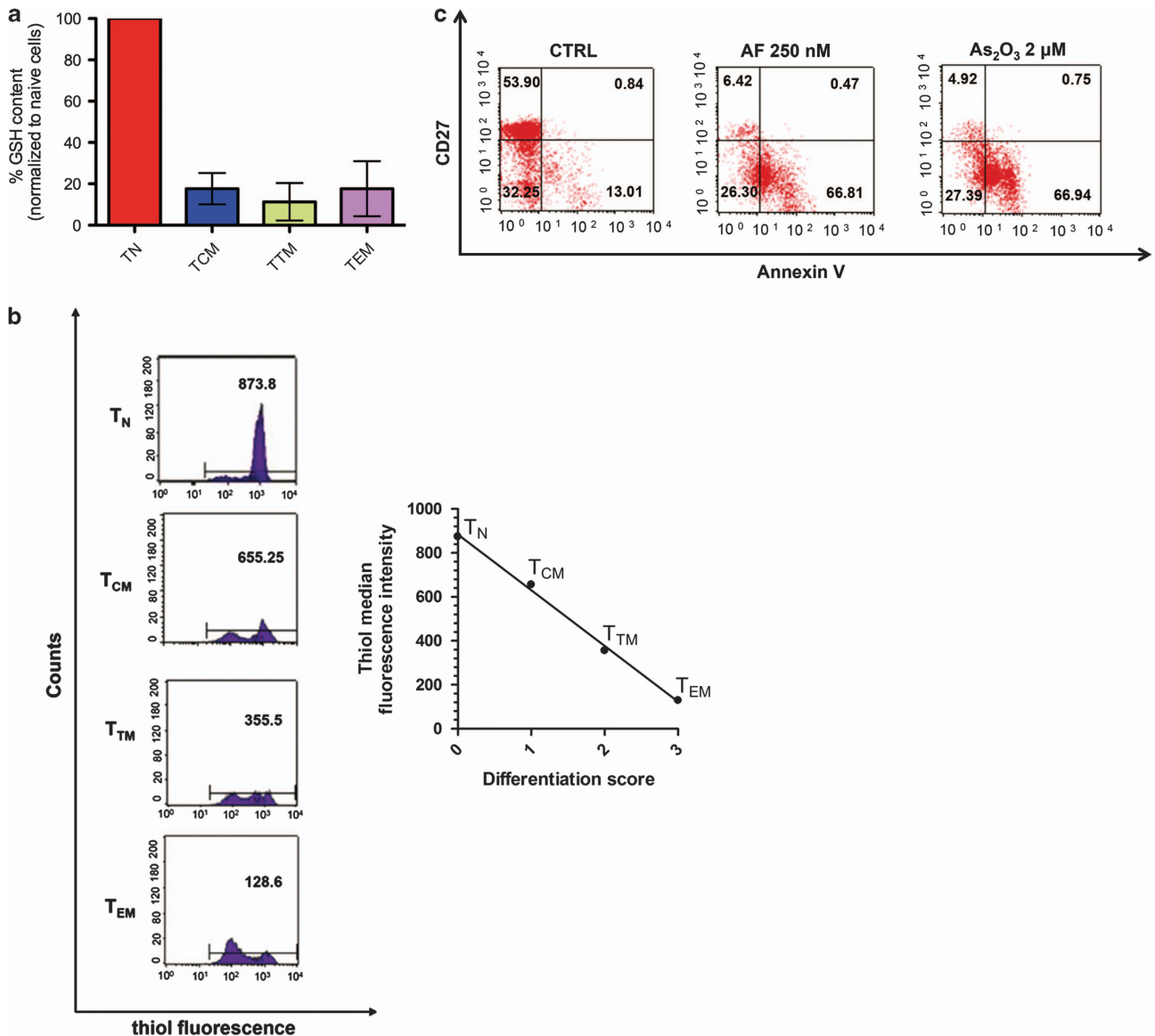
4

Figure 2 Baseline antioxidant levels in sorted CD4$^+$ T-cell subpopulations reflect their susceptibility to AF. (**a**) Total GSH levels in sorted CD4$^+$ T-cell subpopulations. CD4$^+$ T-cell subpopulations were separated by sorting and baseline GSH levels were measured. Data points represent the means from three independent experiments normalized to T$_N$ cells. Data are shown as median ± interquartile range ($n = 3$; $P < 0.001$; repeated measures ANOVA). (**b**) Total thiol content in sorted CD4$^+$ T-cell subpopulations. The thiol content was measured, in all CD4$^+$ T-cell subpopulations, by FACS after labeling cells with ThiolTracker violet dye. The data displayed in both the dot plot and the x, y graph are expressed as the median of fluorescence intensity. On the 'x' axis of the x, y graph, the level of CD4$^+$ T-cell differentiation was associated, for clarity purposes, to an increasing score ranging from 0 to 3 (0 = T$_N$; 1 = T$_{CM}$; 2 = T$_{TM}$; 3 = T$_{EM}$; $P < 0.05$; Spearman's correlation test). (**c**) Replication of the effects of AF on CD4$^+$ T cells by the TrxR inhibitor arsenic trioxide (As$_2$O$_3$). The dot plots show the effect of AF and As$_2$O$_3$ on total CD4$^+$ T cells after 48 h of treatment, analyzed by CD27 (y axis) and Annexin V (x axis) staining. The dot plot shows data from one representative experiment out of three with similar results

differentiation, the level of the effector caspases 3 and 9 was increased in the most differentiated subsets (Figure 5c).

That AF also has a potential impact on reducing lymphocyte proliferation (and, hence, reservoir expansion) is shown by the fact that the cell cycle associated protein Ki67 was decreased in all three long-lived subsets (Figure 5c). Whereas T$_{CM}$ and T$_{TM}$ cells reacted to AF administration also downregulating CD25, that is, the α-chain of the receptor for interleukin-2 (IL-2), a well-known mitogenic and anti-apoptotic cytokine, T$_N$ cells compensated the AF-induced Ki67 downregulation by upregulating CD25. These results point to different mechanisms by which the T$_N$ and T$_{CM}$/T$_{TM}$ subsets react to the AF-induced stress and that may be responsible for the different *in vivo* susceptibility of these cell compartments to AF-induced apoptosis.[7]

AF induces a burst in intracellular peroxide levels within CD4$^+$ T cells. Given the ability of AF to increase the levels of MnSOD, we analyzed reactive oxygen species (ROS) following treatment with AF. To this aim, we measured, by flow cytometry, the levels of dihydrorhodamine (DHR), a compound that becomes fluorescent upon oxidation by intracellular peroxides such as hydrogen peroxide, one well-known cell-death-inducing
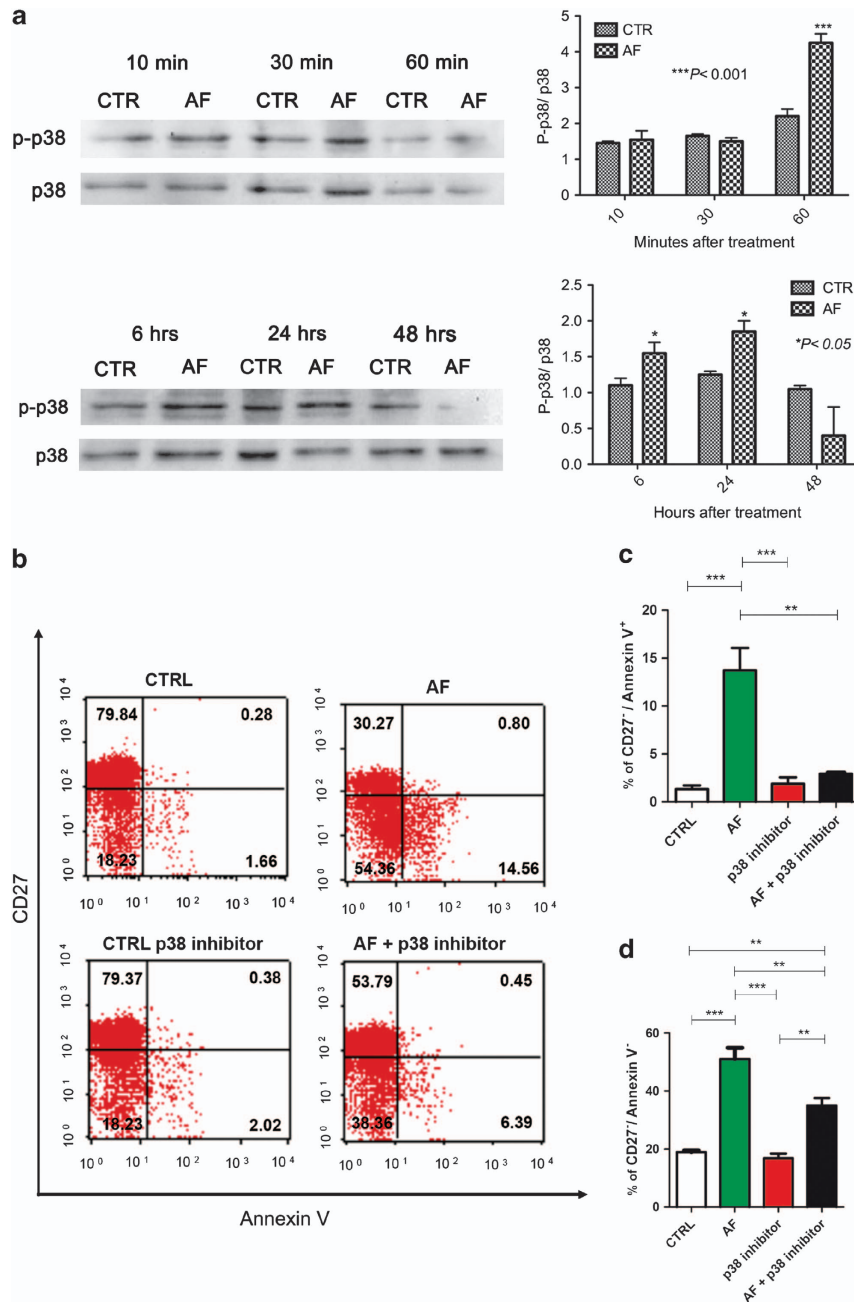
Figure 3 Role of p38 MAPK in the pro-differentiating and pro-apoptotic effects of AF. (**a**) Activation of p38 MAPK by AF treatment. CD4$^+$ T cells were incubated with 250 nM AF for 0–48 h. Protein extracts were prepared at the indicated time points and analyzed on western blot probed with specific antibody against the phosphorylated form of p38 MAPK (p-p38; Tyr182). Loading was controlled with an antibody against total p38 MAPK on the according blot. Respective bands were quantified using Quantity One software and relative p38 MAPK activation was calculated and normalized to the loading control. The blot is shown from one representative experiment out of the two performed. Data in densitometric analysis are graphed as means ± s.d. of the two experiments performed (donors: $n = 2$; *$P < 0.05$; ***$P < 0.001$; one-tailed Student's t-test). (**b**) Effect of AF and the p38 MAPK inhibitor SB203580 on CD27 and Annexin V staining in human CD4$^+$ T cells after 48 h of treatment. The dot plot shows data from one representative experiment out of three (similar results). (**c**) Percentages of CD27$^−$/Annexin V$^+$ CD4$^+$ T cells after 48 h of treatment with AF and SB203580. Data are shown as means ± s.d. (n of donors = 3; *$P < 0.05$; **$P < 0.01$; ***$P < 0.001$; Newman–Keuls post-hoc test following repeated measures ANOVA and LOGIT transformation). (**d**) Percentages of CD27$^−$/Annexin V$^−$ T cells after 48 h of treatment. Data are shown as means ± s.d. (n of donors = 3; *$P < 0.05$; **$P < 0.01$; ***$P < 0.001$; Newman–Keuls post-hoc test following repeated measures ANOVA and LOGIT transformation)

agent.[33,34] As shown in Figure 6a, AF only moderately increased intracellular peroxides levels until 48 h of treatment, at which a major burst was observed (Figures 6a and b).

It is well known that the cytocidal effects of hydrogen peroxide are mediated by ROS following its degradation through the iron-catalyzed Fenton reaction.[35] In line with this view, the iron-containing drug ferroquine greatly enhanced AF-mediated cell death, although the iron compound was per se unable to carry out AF-like effects (data not shown).
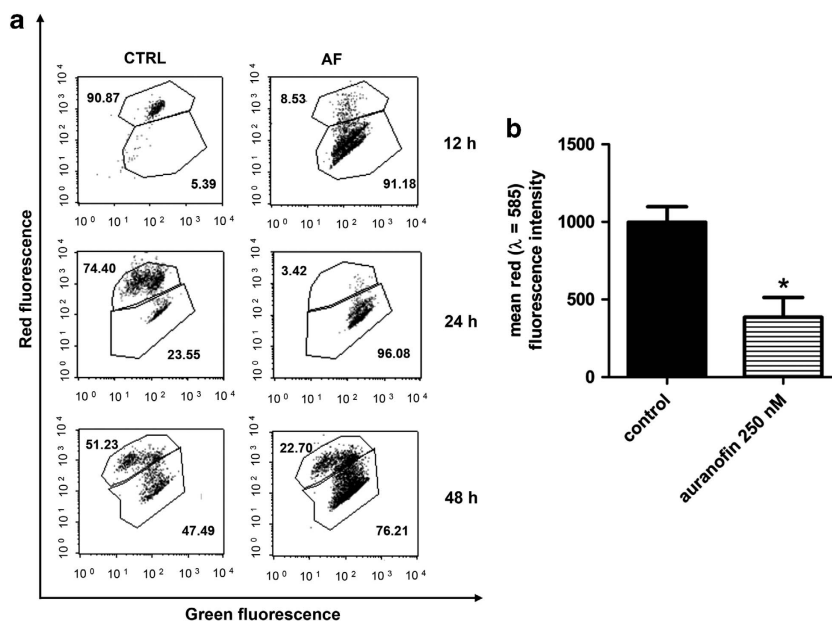
Figure 4 Analysis of MMP ($\Delta\psi m$) in CD4$^+$ T cells after AF treatment. Cells were stimulated with AF for 12–48 h and stained with the JC-1 probe. After staining with JC-1, live cells display red fluorescence (high MMP), whereas apoptotic cells display intermediate or green fluorescence (low MMP). Note that the relatively high rates of cells displaying low MMP observed in the controls are in line with a spontaneous trend to undergo apoptosis in the memory compartment of non-stimulated CD4$^+$ T cells (see Figure 1). (a) Dot plots of red and green fluorescence at 12, 24 and 48 h. (b) Histograms showing the decrease in mean red fluorescence intensity induced by auranofin at 48 h. Data are shown as mean ± s.d. ($n = 4$; *$P < 0.05$; two-tailed paired Student's t-test)

To further test whether the cell-death-promoting effects of AF might be mediated by the production of hydrogen peroxide, we treated the CD4$^+$ T cells with pyruvate, that is, the principal scavenger of hydrogen peroxide (Figure 6c). Pyruvate significantly prevented AF-induced Annexin V stainability but did not inhibit downregulation of CD27 (Figures 6d and e). Interestingly, apart from showing the involvement of hydrogen peroxide in the AF-mediated apoptosis of CD4$^+$ T cells, these results show that the pro-apoptotic and pro-differentiating effects of AF can be de-coupled.

AF displays pro-differentiating effects that are not confined to CD27 downregulation. Among the panel of antigens that we used to define the stage of T-cell differentiation, AF induced downmodulation of CD27 but not of CCR7 (data not shown). CD27$^-$ CCR7$^+$ cells have been described previously, although their role in vivo is not yet known.[8] To elucidate whether the pro-differentiating effect of AF was confined to downmodulation of CD27, we verified the extent of downregulation of CD28, another common marker of the long-lived phenotypes T$_N$, T$_{CM}$ and T$_{TM}$. We found that AF downregulated CD28 expression similarly to CD27, suggesting that AF exerts a true pro-differentiating effect in human CD4$^+$ T cells (Supplementary Figure S3).

AF induces phenotype changes in CD4$^+$ T cells from HIV-infected patients. The pro-differentiating effects of AF were eventually confirmed in CD4$^+$ T cells isolated from three HIV$^+$ patients under ART. Treatment of these cells with AF for 2 days induced a significant reduction in the frequency of the long-lived T$_{CM}$ cells accompanied by a relative increase in the frequency of T$_{EM}$ cells (Figure 7).

AF, however, did not induce viral emergence from latency in CD4$^+$ T cells isolated from HIV-1$^+$ individuals following 3 days of treatment (data not shown).

Discussion

We here show that AF promotes differentiation and apoptosis of the memory CD4$^+$ T-cell subsets that encompass the HIV-1 reservoir. This potential anti-reservoir mechanism is novel and different from the currently investigated 'shock and kill' strategies for HIV reservoir elimination, in that the latter are aimed at inducing viral replication in latent viral reservoirs (which cannot be recognized by drugs or the immune system), whereas AF can shorten the lifespan of the viral reservoirs, favouring their elimination. In this regard, AF-based strategies do not present the risk of enhancing viral replication in HIV$^+$ patients. The pro-apoptotic and pro-differentiating effects of AF were also observed in another cell subpopulation, the central memory CD8$^+$ T cells, the expansion of which is associated with progression to AIDS.[25] High proportions of memory CD8$^+$ T cells are also associated with anergy in SIV-infected macaques, and, therefore, their elimination by AF may explain the improved immune responses associated with control of viral load that we previously observed in SIV-infected macaques following suspension of AF containing therapies.[11, 12] Alternatively, it is also possible that only the pro-differentiating effect of AF contributed to the strong CD8-based immunity, which we observed after treatment interruption, and that death of CD8$^+$ T cells is a so-far inevitable by-product of this strategy.

A major finding of the present study is that the viral reservoir-harbouring CD4$^+$ T$_{CM}$/T$_{TM}$ cells display an overall antioxidant defense lower than that of T$_N$ cells, thus
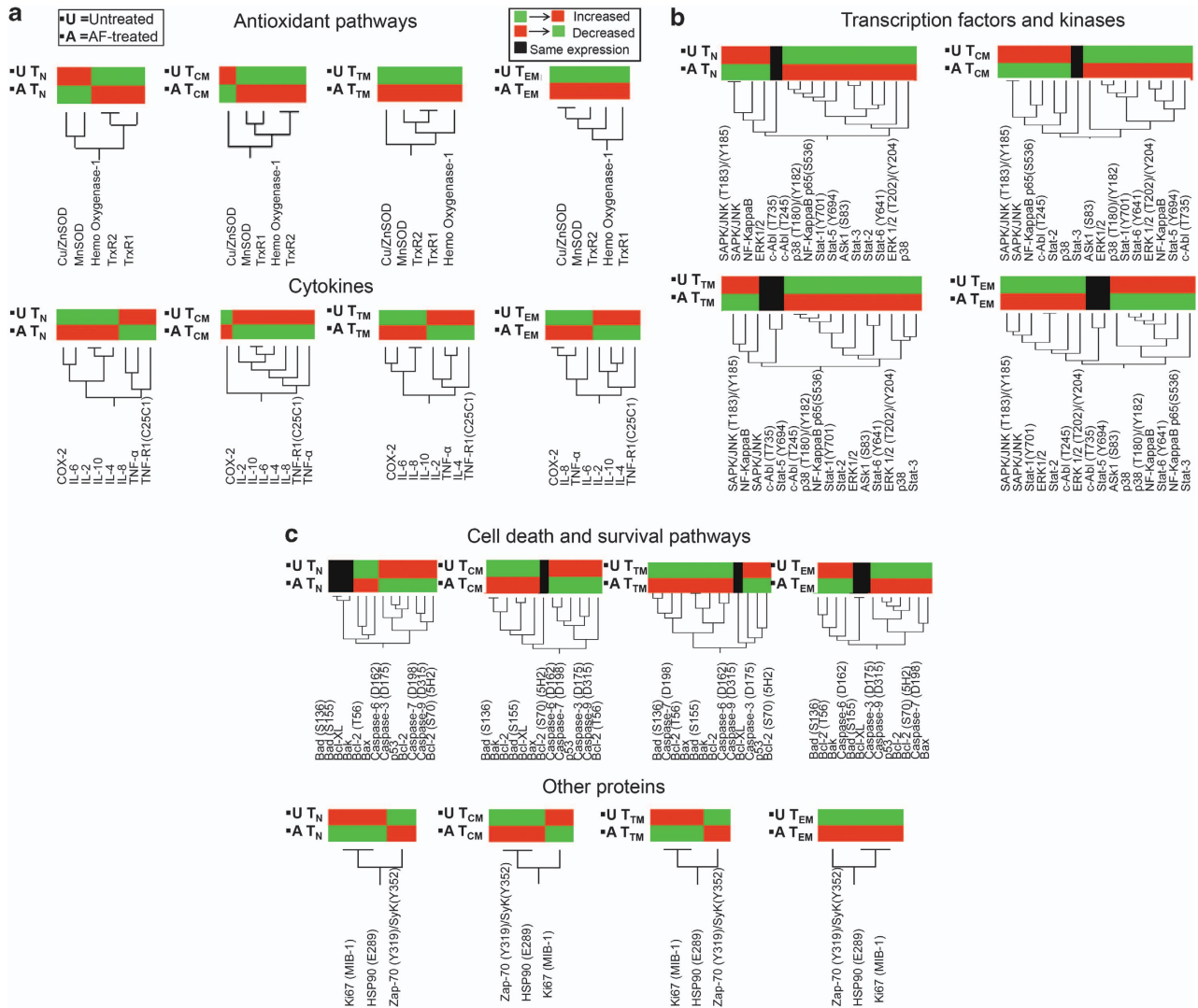
Figure 6 The role of ROS in AF-induced cell death and differentiation. (**a**) ROS production in CD4 $^+$ T cells. ROS content was measured by flow cytometry after labeling cells with 1,2,3 DHR. The dot plot shows ROS fluorescence in total CD4 $^+$ T cells at different time points. (**b**) Histograms showing median intensity of the DHR fluorescence of CD4 $^+$ T cells from three independent experiments. Data are shown as mean ± s.d. (**P < 0.01; Bonferroni's *post-hoc* test following two-way ANOVA). (**c**) Effect of pyruvate, a scavenger of peroxide, on AF-induced cell death and differentiation. Dot plots show CD27 (*y* axis) and Annexin V (*x* axis) staining of human CD4 $^+$ T cells after 48 h of treatment. (**d**) Histogram showing the percentages of CD27 $^-$/Annexin V $^+$ T cells after 48 h of treatment from three independent experiments. Data are shown as means ± s.d. (*P < 0.05; **P < 0.01; ***P < 0.001; Newman–Keuls *post-hoc* test following repeated measures ANOVA and *LOGIT* transformation). (**e**) Percentages of CD27 $^-$/Annexin V $^-$ T cells after 48 h of treatment from three independent experiments. Data are shown as mean ± s.d. (*P < 0.05; **P < 0.01; ***P < 0.001; Newman–Keuls *post-hoc* test following repeated measures ANOVA and *LOGIT* transformation)
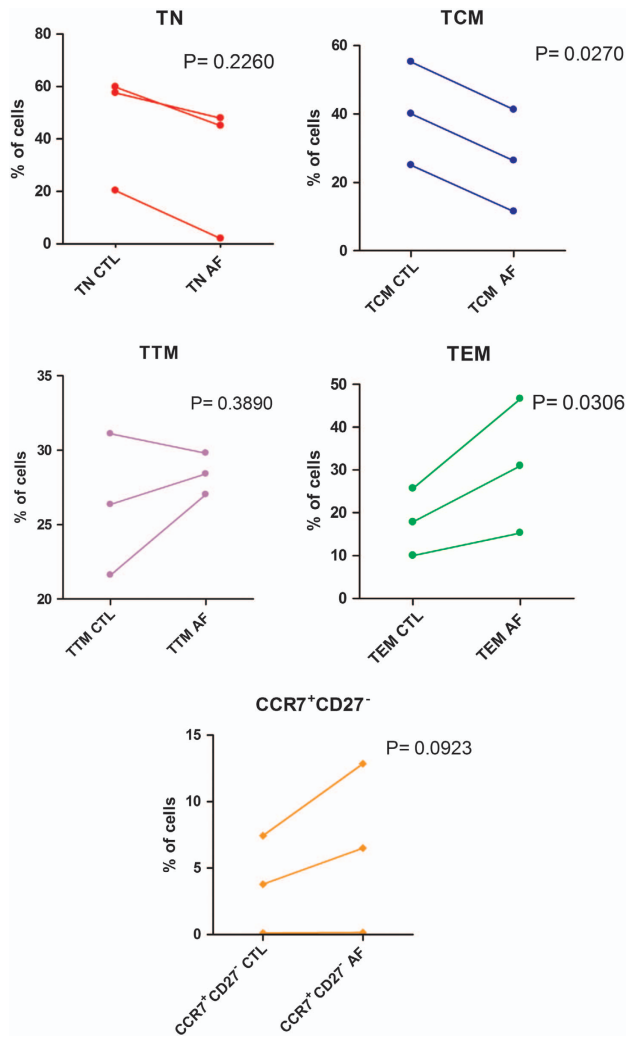
Figure 7 AF-induced phenotype changes in CD4$^+$ T cells from HIV-infected individuals. Shown are the proportions of CD4$^+$ T-cell subpopulations of human HIV$^+$ subjects, under ART, after 2 days of treatment with auranofin. CD4$^+$ T-naive (T$_N$; i.e., CD45RA$^+$ CD27$^+$ CCR7$^+$), CD4$^+$ T-central memory (T$_{CM}$; CD45RA$^-$ CD27$^+$ CCR7$^+$), CD4$^+$ T-transitional memory (T$_{TM}$; CD45RA$^-$ CD27$^+$ CCR7$^-$) and CD4$^+$ T-effector memory (T$_{EM}$; CD45RA$^-$ CD27$^-$ CCR7$^-$), CCR7$^+$ CD27$^-$. The *P*-values are shown, as obtained by paired *t*-test analysis following a *LOGIT* transformation to restore normality

apoptotic and pro-survival signals. AF-mediated inhibition of TrxRs would represent a sparking event in the activation of the apoptotic cascade in human primary CD4$^+$ T cells. This event subsequently activates p38 MAPK, which becomes phosphorylated. It is known that phosphorylation of p38 MAPK is associated with a decrease in the anti-apoptotic potential of the Bcl-2 protein.[45,46] If this reconstruction is correct, p38 MAPK activation would in turn induce mitochondrial depolarization and caspase activation leading to cell death. The eventual cell death observed suggests that this pathway is able to overcome a likely AF-induced pro-survival signal emerging from our protein array analysis. This signal involves Erk1/2 and likely results in the phosphorylation of Bad in S136/ S155, hampering its dimerization with BclXL (Figure 5c).

Our data also show that the pro-differentiating effect of AF can be de-coupled from the pro-apoptotic effect. Differently

from the pro-apoptotic effect, the pro-differentiating effect of AF is not hydrogen peroxide dependent, as evidenced by the lack of inhibition by pyruvate of the AF-induced CD27 downmodulation. The pro-differentiating pathway is likely to diverge from the pro-apoptotic pathway downstream of p38 MAPK activation. In this regard, activation of ZAP70/Syk, a pivotal mediator of lymphocyte activation and differentiation, represents a possible explanation for the pro-differentiating effects of AF.[47] Ingenuity Pathway Analysis results support several possibilities for ZAP70/Syk activation as a consequence of pathways activated by AF (Supplementary Figure S4). Unfortunately, our experiments using the ZAP70/Syk inhibitor (Piceatannol, Sigma-Aldrich, St Louis, MO, USA) were hampered by the extremely high toxicity of the compound starting from 24 h of incubation (data not shown). The pro-differentiating effect of AF may have an important role in viral reservoir restriction *in vivo*, limiting the 'stem-cell-ness' of the T$_{CM}$ and T$_{TM}$ pools, and turning these cells into short-lived lymphocytes with limited *in vivo* persistence of the associated viral reservoir. Further investigation of these mechanisms, for example, through RNA macro-array analysis, might open new avenues for novel therapeutic strategies aimed at broader and more ambitious targets, such as complete eradication of lentiviral infections.

Materials and Methods

Cell sorting and flow cytometric analysis. Low-density mononuclear cells (less than 1,077 g/mL) were isolated by Ficoll-Hypaque density-gradient centrifugation (Sigma-Aldrich). Human peripheral blood mononuclear cells (PBMCs) were isolated from whole blood by Ficoll centrifugation and resuspended in RPMI-10% fetal bovine serum (FBS). CD4$^+$ T cells were isolated by positive selection (MACS Separation Columns, Miltenyi Biotec, Teterow, Germany). Isolated CD4$^+$ T cells (purity: >90%) were stained for 20 min at 4 °C in MACS buffer (PBS-1,25%FBS, 2 mM EDTA) with the following combination of antibodies: CD45RO-FITC-conjugated antibody (Becton Dickinson (BD), Franklin Lakes, NJ, USA), CD27-PE-conjugated antibody (Miltenyi Biotec, Bergisch Gladbach, Germany) and CCR7-PE Cy7-conjugated antibody (BD). Cells were washed in MACS buffer before being resuspended at 30×10^6 cells per mL in the same buffer for sorting. Cell subpopulations (T$_N$, T$_{CM}$, T$_{TM}$ and T$_{EM}$; purity: >98%) were sorted on a BD fluorescence-activated cell sorting (FACS) Aria, (Becton-Dickinson, San Jose, CA, USA). Debris and cell doublets were gated out on the basis of physical parameters. CD45RO$^+$ and CD45RO$^-$ lymphocytes were then selected after analyzing single-cell events in a FITC *versus* FSC plot. The gated CD45RO$^+$ T-cell events were then plotted for CD27 *versus* CCR7 expression, which allows the selection of the T$_{CM}$, T$_{TM}$ and T$_{EM}$ subpopulations, whereas the gated CD45RO$^-$ T-cell events were plotted for CD27 *versus* CCR7 expression and the cells positive for both markers were sorted as T$_N$. Purity of the sorted populations was assessed by flow cytometry with a FACSCanto flow cytometer (Becton-Dickinson) and analyzed with the FACS Diva software (Becton-Dickinson).

Total CD4$^+$ T cells and isolated subsets were cultured at 1×10^6 cells/mL in RPMI supplemented with 10% FBS and IL-2. Cells were incubated with AF (250 nM) and with or without different compounds aimed at enhancing/inhibiting or mimicking the effect of AF: p38 MAPK inhibitor (20 μM; SB203580 Calbiochem, La Jolla, CA, USA), Erk1/2 inhibitor (20 μM, PD98059 Calbiochem), pyruvate (1 mM), As$_2$O$_3$ (2 μM) and ZAP70/Syk inhibitor (piceatannol, P0453 Sigma-Aldrich). After 48 h of culture, cells were collected and stained for memory and activation markers using the following combination of antibodies and reagents: CD45RO-FITC (BD) and CD27-PE (BD) in combination with Annexin V staining (Sigma-Aldrich). Cells were stained for 20 min at 4 °C in MACS buffer and washed in the same buffer before acquisition. 200 000 events were collected during flow cytometric analysis on a FACSCalibur flow cytometer (Becton-Dickinson) and analyzed using the CellQuest Pro software (BD).

Measurement of GSH. Intracellular GSH was measured with the Glutathione assay kit (Sigma-Aldrich, Milan, Italy) according to manufacturer's instructions. The
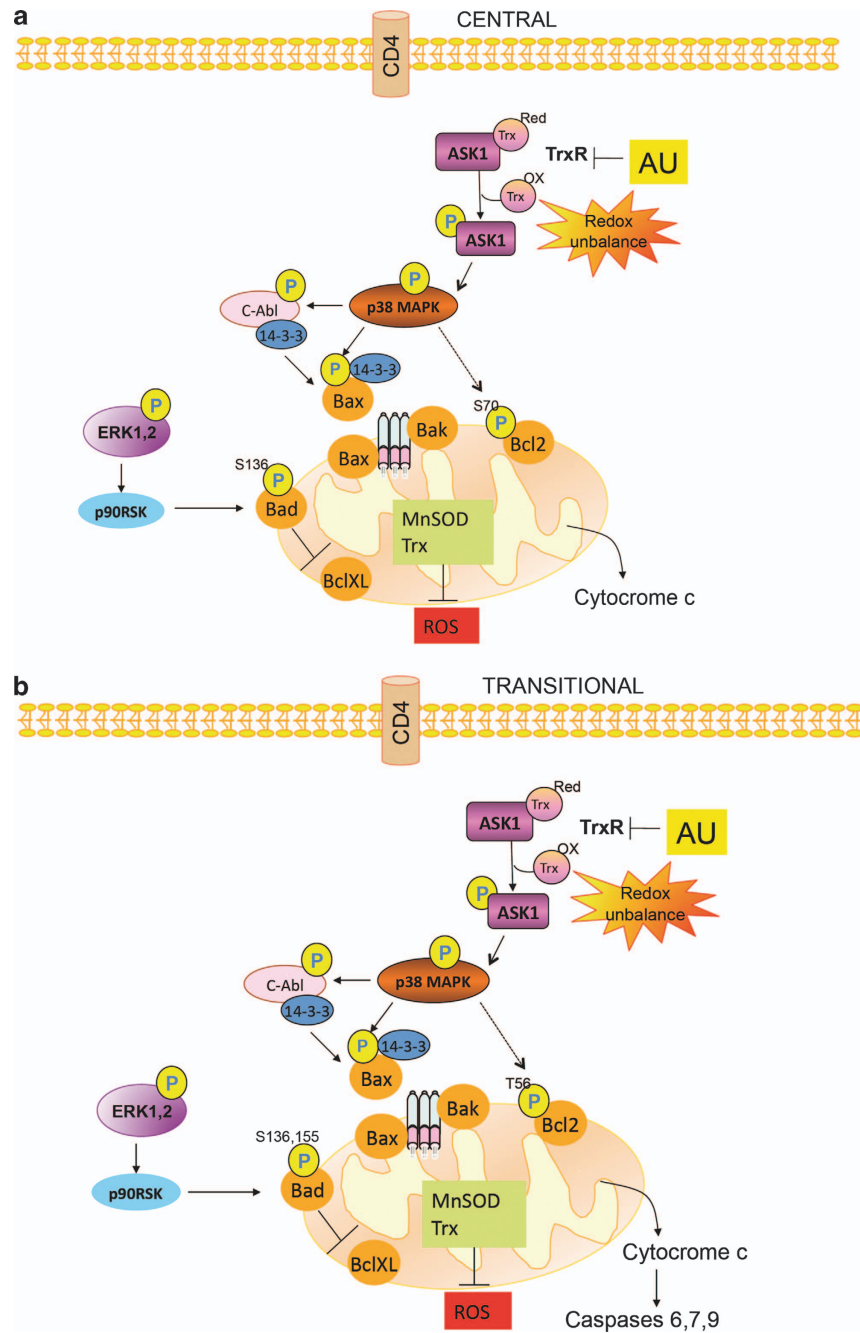
Figure 8 (**a** and **b**) Proposed model of the molecular mechanisms underlying AF-induced apoptosis of human primary CD4 $^+$ central and transitional memory T cells

samples were first deproteinized with the 5% 5-sulfosalicylic acid solution and their GSH content was then measured using a kinetic assay. Briefly, in this assay, catalytic amounts of GSH cause a continuous reduction of 5,5′-dithiobis-(2-nitrobenzoic) acid (DTNB) to TNB. The quantity of TNB produced in the reaction is measured at 412 nm, although the oxidized GS-TNB product arising from the reaction is recycled to GSH by GSH-reductase and NADPH. Values were expressed as nanomoles of GSH per milligram of protein in the original cell extract.

Measurement of thiol content. The thiol content was measured using a ThiolTracker Violet dye (10 μM; T10095, Invitrogen Molecular Probes). The staining was performed by applying the dye directly to live cells (500 000 cells) in thiol-free buffer for 30 min in the dark at 37 °C. 200 000 events were subsequently analyzed using a flow cytometer at 405 nm excitation as described by the manufacturer.

Detection of MMP (Δψm). MMP was estimated by flow cytometry after staining with the JC-1 fluorescent dye (M34152, MitoProbe JC-1 Assay Kit, Life Technologies, Grand Island, NY, USA). 500 000 cells were treated with AF for 12, 24 and 48 h, harvested and then washed with cold PBS, and incubated with JC-1 solution (2.5 μg/mL) for 30 min in the dark at 37 °C. Following incubation, cells were washed twice with cold PBS and resuspended in 200 μL of cold PBS. Immediately after resuspension, the fluorescence emitted by JC-1 was analyzed by flow cytometry (FACSCalibur). 200 000 events were collected during flow cytometric analysis and analyzed using the CellQuest Pro software (BD). High MMP characterizes cells in the normal (live) state and favours the formation of JC-1 aggregates that predominantly yield red fluorescence (~590 nm). Reduced MMP characterizes cells in the apoptotic state and favours the maintenance of monomeric JC-1 that yields green fluorescence (~529 nm). Thus, a red to green switch in fluorescence indicates a decrease in the MMP.

Western blot analysis. Cell lysates extracted from 1×10^6 cells were resuspended in reducing SDS sample buffer, separated on SDS–polyacrylamide gels, and blotted onto nitrocellulose membranes. The membranes were blocked with 10% nonfat dry milk in TBS-tween for 1 h at room temperature. The activation of p38 MAPK was detected with phospho-specific rabbit monoclonal antibody (1/500, Santa Cruz Biotechnology, Inc., Santa Cruz, CA, USA). After stripping of bound antibody, loading was controlled with an antibody against p38 MAPK using rabbit polyclonal antisera (1/500, Santa Cruz Biotechnology, Inc.) on the according blot, as described inref. 48. Anti-rabbit IgG horseradish-peroxidase–conjugated antibody (1/5000, Jackson ImmunoResearch Laboratories, West Grove, PA, USA) was applied for visualization. Blots were developed with an enhanced chemiluminescence system (GE Healthcare, Milan, Italy). Respective bands were quantified using Quantity One software (Bio Rad Laboratories, Hercules, CA, USA), and relative p38 MAPK activation was calculated and normalized to the loading control.

Reverse phase protein microarray analysis. Samples were printed on glass-backed nitrocellulose array slides using an Aushon 2470 arrayer (Aushon BioSystems, Burlington, MA, USA) equipped with 350 μm pins as previously described.[49] Sample lysates were printed on 50 nitrocellulose slides and subjected to reverse phase protein microarray analysis (RPMA). Each sample was printed in triplicate. Slides 15 and 25 were then stained with Sypro Ruby Protein Blot Stain (Molecular Probes, Eugene, OR, USA) and visualized with NovaRay Image Acquisition Software (Alpha Innotech, San Leandro, CA, USA) to determine the total protein concentration. Before antibody staining, the slides were treated with Reblot antibody stripping solution (Chemicon, Temecula, CA, USA) and incubated for 5 h at room temperature in blocking solution with constant shaking. Blocked slides were stained with 43 different antibodies targeting total and phosphorylated proteins using an automated stainer (Dako Cytomation, Carpinteria, CA, USA). Each antibody was subjected to rigorous validation for single band specificity at the correct molecular weight (MW) by western blotting along with the use of appropriate ligand-induction controls for phospho-specific antibodies. Catalyzed Signal Amplification System kit (Dako Cytomation) and fluorescent IRDye 680 Streptavidin (LI-COR, Lincoln, NE, USA) were used as detection system. Stained slides were scanned with NovaRay Image Acquisition Software (Alpha Innotech).

Acquired images of each slide were analyzed using MicroVigene software (Vigenetech, Carlisle, MA, USA), which finds spots, performs local background subtraction, averages replicates and normalizes each sample for the total protein value. Normalization between slides was performed using control cell lysate printed on each slide as a bridging case (Supplementary Figure S5).

Systems biology. Ingenuity Pathway Analysis (IPA7.0, Ingenuity System, http://www.ingenuity.com/) was used to establish physical and/or functional interactions among proteins found either upregulated or downregulated in AF-induced CD4$^+$ T-cell subpopulations (T_N, T_{CM}, T_{TM} and T_{EM}).

Cell separation and isolation of CD4$^+$ T-cell subsets from HIV$^+$ subjects by cell sorting. PBMCs from HIV$^+$ subjects were isolated from whole blood by density gradient centrifugation (Ficoll) and resuspended in RPMI/10% FBS. Total CD4$^+$ T cells were isolated by negative selection on a Robosep (Stemcell–Human CD4+ T cell enrichment kit). Isolated CD4$^+$ T cells (more than 90% pure, as determined by flow cytometry) from HIV$^+$ subjects were then sorted on an ARIA II (BD Biosciences) into T_N (CD45RA$^+$CD27$^+$CCR7$^+$), T_{CM} (CD45RA$^-$CD27$^+$CCR7$^+$), T_{TM} (CD45RA$^-$CD27$^+$CCR7$^-$) and T_{EM} (CD45RA$^+$CD27$^-$CCR7$^-$) using the following combination of antibodies: CD3-PB, CD4-A700, CD45RA-APC Cy7, CD27-PE, CCR7-PE Cy7 and Vivid-AmCyan (Invitrogen Life Technologies, Carlsbad, CA, USA). Sorted subsets were more than 98% pure.

Cell culture. Total CD4$^+$ T cells or isolated subsets, obtained from HIV$^+$ subjects, were cultured from 1 to 5×10^6 cells/mL in RPMI completed with 10% FBS for 3 to 6 days in the presence or absence of increasing concentrations of AF ranging from 0 to 500 nM.

Reactivation assays and HIV-1 viral RNA quantification. The virus was pelleted by centrifugation for 60 min at 17 000 r.p.m. at 4 °C. To generate the standard curve, a sample of titer-known ACH2 virus was pelleted in the same run. After the centrifugation, total viral RNA was extracted with the QIAamp viral RNA extraction kit from Qiagen (Crawley, UK) according to the manufacturer's instructions. Briefly, samples were lysed under highly denaturing conditions to

inactivate RNases. Alcohol was added and lysates loaded onto the QIAamp spin column. Wash buffers were used to remove impurities and pure, ready-to-use RNA was then eluted in 60 μL of low-salt buffer (supplied with the kit). The RNA solution was stored at -80 °C until use.

The purified RNA was then used as a matrix for a two-step quantitative real-time reverse transcription-PCR (RT-PCR followed by qRT-PCR). For each sample, a minimum of two independent replicates (separate wells) were performed, including the ACH2 RNA sample as a standard ranging from 300 000 copies to 3 copies.

Reverse transcription (RT-PCR): Total viral RNA (17 μL) was first treated with 1 U DNase in DNase I reaction buffer $1 \times$ for 10 min at 25 °C. The DNase was inactivated with 1 μL 25 mM EDTA for 10 min at 65 °C. Total viral RNA was then reverse-transcribed into complementary DNA for qPCR analysis. RT-PCR was performed in 50 μL of solution containing 22 μL of DNase-treated RNA, 0.5 μL of each gag gene-specific primers (50 μM each), LM667 (5′-ATG CCA CGT AAG CGA AAC TCT GGC TAA CTA GGG AAC CCA CTG-3′) and GagR (5′-AGC TCC CTG CTT GCC CAT A-3′), 2 μL of Superscript III RT/Platinum Taq mix and $1 \times$ Reaction mix (RT-PCR One Step kit – Invitrogen) in a final 50 μL volume. No-template samples were used as negative controls. The running conditions were as follows: reverse transcription 30 min at 50 °C, denaturation 2 min at 94 °C followed by 20 cycles of 94 °C for 15 sec (denaturation), 62 °C for 30 s (annealing) and 68 °C for 1 min (extension). The reaction was achieved by a final elongation at 68 °C for 5 min before cooling gradually to 4 °C. The cDNAs were diluted 10-fold with DNase–RNase-free water, then subjected to quantitative real-time PCR analysis.

Quantitative real-time PCR: Experiments were performed with a LightCycler Carousel-based system (Roche, Penzberg, Germany). H_2O was included as a no-template control. All reactions were carried out in 20 μL of reaction mixtures containing 6.4 μL of cDNAs, 0.3 μL of Taq DNA polymerase (Invitrogen), 1X Jumpstart mix (Sigma), 1.8 μL MgCl$_2$ 25 mM, 0.25 μL of each gag gene-specific primers (100 μM each), Lambda T (5′-ATG CCA CGT AAG CGA AAC T-3′) and A55M (5′-GCT AGA GAT TTT CCA CAC TGA CTA A-3′), 0.5 μL each hybridization probes (8 μM each) LTR-LC (LCred640-5′-CAC TCA GGG CAA GCT TTA TTG AGG C-3′-Phosphate) and LTR-FL (5′-CAC AAC AGA CGG GCA CAC ACT ACT TGA-3′-Fluorescein). The running conditions were as follows: 4 min at 95 °C, followed by 50 cycles of 95 °C for 10 sec (denaturation), 60 °C for 10 sec (annealing) and 72 °C for 9 sec (extension). Following the PCR reaction, melting curve analysis was performed to control amplification specificity by measuring the fluorescence intensity across the temperature interval from 45 °C to 95 °C. The absence of nonspecific products or primer dimers was indicated by observation of a single melting peak in melting curve analysis.

Statistical analyses. Statistical analyses were conducted using GraphPad Prism, v5.0 (GraphPad software, La Jolla, CA, USA), unless otherwise specified. Correlation between two variables was analyzed using Spearman's correlation coefficients (r). Differences between variables were analyzed using parametric tests such as *t*-tests, or, in case of multiple comparisons, one- or two-way analysis of variance (ANOVA) followed by an appropriate *post-hoc* test. Paired or repeated measures tests were adopted for matched observational data points. An appropriate transformation such as the *LOGIT* transformation of percentage values was done to restore normality, where necessary. A *P*-value < 0.05 was considered to be statistically significant.

Conflict of Interest

The Istituto Superiore di Sanità has requested patent rights on the use of auranofin for treatment of HIV/AIDS.The authors declare no conflict of interest.

Author contributions

AS, ATP and EG conceived the study. AS designed the experiments, analyzed the data, drafted the manuscript and directed the study; ATP and EG codirected the study; BC conducted the *in vitro* experiments and participated at data analysis, manuscript drafting, experimental design and project coordination; RS conducted *in vitro* experiments on intracellular signaling, contributed to data analysis and interpretation of the molecular mechanism; SDF and NC conducted the experimental design and the *ex vivo* analyses of cells from HIV[+] patients; ILS and SN contributed preliminary work and ideas on which this report is based; DA and BD (from Dr. Jonathan Karn's laboratory) conduced the Ingenuity Pathway Analysis; AB conducted the cell sorting; EP cultivated the stem cells; DL, LL and PEIII conducted the RPMA.

1. Badley AD, Sainski A, Wightman F, Lewin SR. Altering cell death pathways as an approach to cure HIV infection. *Cell Death Dis* 2013; **4**: 718.
2. Lafeuillade A. Eliminating the HIV reservoir. *Curr HIV/AIDS Rep* 2012; **9**: 121–131.
3. Remoli AL, Marsili G, Battistini A, Sgarbanti M. The development of immune-modulating compounds to disrupt HIV latency. *Cytokine Growth Factor Rev* 2012; **23**: 159–172.
4. Monforte AD, Svicher V, Nozza S, Lazzarin A, Marchetti G, Perno CF. Highlights on HIV eradication in 2013. *AIDS* 2013 [Epub ahead of print].
5. Savarino A, Garaci E. Therapeutic imprinting of the immune system: towards a remission of AIDS in primates? *Retrovirology* 2012; **9**: 75.
6. Palmer S, Josefsson L, Coffin JM. HIV reservoirs and the possibility of a cure for HIV infection. *J Intern Med* 2011; **270**: 550–560.
7. Lewis MG, Dafonseca S, Chomont N, Palamara AT, Tardugno M, Mai A et al. Gold drug auranofin restricts the viral reservoir in the monkey AIDS model and induces containment of viral load following ART suspension. *AIDS* 2011; **25**: 1347–1356.
8. Chomont N, El-Far M, Ancuta P, Trautmann L, Procopio FA, Yassine-Diab B et al. HIV reservoir size and persistence are driven by T cell survival and homeostatic proliferation. *Nat Med* 2009; **15**: 893–900.
9. Chomont N, DaFonseca S, Vandergeeten C, Ancuta P, Sékaly RP. Maintenance of CD4 + T-cell memory and HIV persistence: keeping memory, keeping HIV. *Curr Opin HIV AIDS* 2011; **6**: 30–36.
10. Finzi D, Blankson J, Siliciano JD, Margolick JB, Chadwick K, Pierson T et al. Latent infection of CD4 + T cells provides a mechanism for lifelong persistence of HIV-1, even in patients on effective combination therapy. *Nat Med* 1999; **5**: 512–517.
11. Shytaj IL, Norelli S, Chirullo B, Della Corte A, Collins M, Yalley-Ogunro J et al. A highly intensified ART regimen induces long-term viral suppression and restriction of the viral reservoir in a simian AIDS model. *PLoS Pathog* 2012; **8**: e1002774.
12. Shytaj IL, Chirullo B, Wagner W, Ferrari MG, Sgarbanti R, Corte AD et al. Investigational treatment suspension and enhanced cell-mediated immunity at rebound followed by drug-free remission of simian AIDS. *Retrovirology* 2013; **10**: 71.
13. Eisler R. Chrysotherapy: a synoptic review. *Inflamm Res* 2003; **52**: 487–501.
14. Friker SP. Medical uses of gold compounds: past, present and future. *Gold Bull* 1996; **29**: 53–59.
15. Sutton BM. Gold compound for rheumatoid arthritis. *Gold Bull* 1986; **19**: 15–16.
16. Kean WF, Hart L, Buchanan WW. Auranofin. *Br J Rheumatol* 1997; **36**: 560–572.
17. Hashimoto K, Whitehurst CE, Lipsky PE. Synergistic inhibition of T cell proliferation by gold sodium thiomalate and auranofin. *J Rheumatol* 1994; **21**: 1020–1026.
18. Han S, Kim K, Kim H, Kwon J, Lee YH, Lee CK et al. Auranofin inhibits overproduction of pro-inflammatory cytokines, cyclooxygenase expression and PGE2 production in macrophages. *Arch Pharm Res* 2008; **31**: 67–74.
19. Kim TS, Kang BY, Lee MH, Choe YK, Hwang SY. Inhibition of interleukin-12 production by auranofin, an anti-rheumatic gold compound, deviates CD4(R) T cells from the Th1 to the Th2 pathway. *Br J Pharmacol* 2001; **134**: 571–578.
20. Gromer S, Wissing J, Behne D, Ashman K, Schirmer RH, Flohé L et al. A hypothesis on the catalytic mechanism of the selenoenzyme thioredoxin reductase. *Biochem J* 1998; **332**: 591–592.
21. Rigobello MP, Scutari G, Boscolo R, Bindoli A. Induction of mitochondrial permeability transition by auranofin, a gold(I)-phosphine derivative. *Br J Pharmacol* 2002; **136**: 1162–1168.
22. Rigobello MP, Folda A, Dani B, Menabo R, Scutari G, Bindoli A. Gold(I) complexes determine apoptosis with limited oxidative stress in Jurkat T cells. *Eur J Pharmacol* 2008; **582**: 26–34.
23. Cox AG, Brown KK, Arner ES, Hampton MB. The thioredoxin reductase inhibitor auranofin triggers apoptosis through a Bax/Bak-dependent process that involves peroxiredoxin 3 oxidation. *Biochem Pharmacol* 2008; **76**: 1097–1109.
24. López M, Soriano V, Peris-Pertusa A, Rallón N, Restrepo C, Benito JM. Elite controllers display higher activation on central memory CD8 T cells than HIV patients successfully on HAART. *AIDS Res Hum Retroviruses* 2011; **27**: 157–165.
25. Hazenberg MD, Otto SA, van Benthem BH, Roos MT, Coutinho RA, Lange JM et al. Persistent immune activation in HIV-1 infection is associated with progression to AIDS. *AIDS* 2003; **17**: 1881–1888.
26. Liu C, Liu Z, Li M, Li X, Wong YS, Ngai SM et al. Enhancement of auranofin-induced apoptosis in MCF-7 human breast cells by selenocystine, a synergistic inhibitor of thioredoxin reductase. *PLoS One* 2013; **8**: e53945.
27. Sies H. Glutathione and its role in cellular functions. *Free Radic Biol Med* 1999; **27**: 916–921.
28. Lin S, Del Razo LM, Styblo M, Wang C, Cullen WR, Thomas DJ. Arsenicals inhibit thioredoxin reductase in cultured rat hepatocytes. *Chem Res Toxicol* 2001; **14**: 305–311.
29. McCubrey JA, Lahair MM, Franklin RA. Reactive oxygen species-induced activation of the MAP kinase signaling pathways. *Antioxid Redox Signal* 2006; **8**: 1775–1789.
30. Cobb MH. MAP kinase pathways. *Prog Biophys Mol Biol* 1999; **71**: 479–500.
31. Sugawara T, Moriguchi T, Nishida E, Takahama Y. Differential roles of ERK and p38 MAP kinase pathways in positive and negative selection of T lymphocytes. *Immunity* 1998; **9**: 565–574.
32. Nordberg J, Arnér ES. Reactive oxygen species, antioxidants, and the mammalian thioredoxin system. *Free Radic Biol Med* 2001; **31**: 1287–1312.
33. Wardman P. Fluorescent and luminescent probes for measurement of oxidative and nitrosative species in cells and tissues: progress, pitfalls, and prospects. *Free Radic Biol Med* 2007; **43**: 995–1022.
34. Filomeni G, Piccirillo S, Rotilio G, Ciriolo MR. p38 MAPK and ERK1/2 dictate cell death/survival response to different pro-oxidant stimuli via p53 and Nrf2 in neuroblastoma cells SH-SY5Y. *Biochem Pharmacol* 2012; **83**: 1349–1357.
35. Fenton HJH. Oxidation of tartaric acid in presence of iron. *J Chem Soc* 1894; **65**: 899–910.
36. Cobb MH, Goldsmith EJ. How MAP kinases are regulated. *J Biol Chem* 1995; **270**: 14843–14846.
37. Karin M. The regulation of AP-1 activity by mitogen-activated protein kinases. *J Biol Chem* 1995; **270**: 16483–16486.
38. Ohno K, Han J. The p38 signal transduction pathway activation and function. *Cell Signal* 2000; **12**: 1–13.
39. Filomeni G, Ciriolo MR. Redox control of apoptosis: an update. *Antioxid Redox Signal* 2006; **8**: 2187–2192.
40. Chang KC, Hsu CC, Liu SH, Su CC, Yen CC, Lee MJ et al. Cadmium induces apoptosis in pancreatic β-cells through a mitochondria-dependent pathway: the role of oxidative stress-mediated c-Jun N-terminal kinase activation. *PLoS One* 2013; **8**: e54374.
41. Zhao WX, Tang SS, Jin X, Zhang CM, Zhang T, Wang CC et al. Olaquindox-induced apoptosis is suppressed through p38 MAPK and ROS-mediated JNK pathways in HepG2 cells. *Cell Biol Toxicol* 2013; **29**: 229–238.
42. Kim IS, Jin JY, Lee IH, Park SJ. Auranofin induces apoptosis and when combined with retinoic acid enhances differentiation of acute promyelocytic leukaemia cells *in vitro*. *Br J Pharmacol* 2004; **142**: 749–755.
43. Buettner GR. Superoxide dismutase in redox biology: the roles of superoxide and hydrogen peroxide. *Anticancer Agents Med Chem* 2011; **11**: 341–346.
44. Takahashi A, Hanson MG, Norell HR, Havelka AM, Kono K, Malmberg KJ et al. Preferential cell death of CD8 + effector memory (CCR7-CD45RA-) T cells by hydrogen peroxide-induced oxidative stress. *J Immunol* 2005; **174**: 6080–6087.
45. De Chiara G, Marcocci ME, Torcia M, Lucibello M, Rosini P, Bonini P. Bcl-2 Phosphorylation by p38 MAPK: identification of target sites and biologic consequences. *J Biol Chem* 2006; **281**: 21353–21361.
46. Farley N, Pedraza-Alva G, Serrano-Gomez D, Nagaleekar V, Aronshtam A, Krahl T. p38 mitogen-activated protein kinase mediates the Fas-induced mitochondrial death pathway in CD8 + T cells. *Mol Cell Biol* 2006; **26**: 2118–2129.
47. Weiss A, Littman DR. Signal transduction by lymphocyte antigen receptors. *Cell* 1994; **76**: 263–274.
48. Marjuki H, Alam MI, Ehrhardt C, Wagner R, Planz O, Klenk HD et al. Membrane accumulation of influenza A virus hemagglutinin triggers nuclear export of the viral genome via protein kinase Calpha-mediated activation of ERK signaling. *J Biol Chem* 2006; **281**: 16707–16715.
49. Espina V, Edmiston KH, Heiby M, Pierobon M, Sciro M, Merritt B et al. A portrait of tissue phosphoprotein stability in the clinical tissue procurement process. *Mol Cell Proteomics* 2008; **7**: 1998–2018.

Supplementary Information accompanies this paper on Cell Death and Disease website (http://www.nature.com/cddis)